Conf-9404124--1

LA-UR- 94-818

Title: The Microstructure and Morphology of Carbon Black: A Study using Small angle Neutron Scattering and Contrast Variation

Author(s): Rex P. Hjelm, Jr., Wesley A. Wampler, Philip A. Seeger, and Michel Gerspacher

Submitted to: JOURNAL OF MATERIALS RESEARCH

Los Alamos
NATIONAL LABORATORY

Form No. 836 R5
ST 2629 10/91

The Microstructure and Morphology of Carbon Black: A Study using Small angle Neutron Scattering and Contrast Variation

by

Rex P. Hjelm, Jr. *§, Wesley A. Wampler†, Philip A Seeger § and Michel Gerspacher†

§ Los Alamos Neutron Scattering Center, Los Alamos National Laboratory, Los Alamos, New Mexico 87545-1663, USA

† Sid Richardson Carbon Company, 4825 North Freeway, Fort Worth, Texas, 76106, USA

Send Correspondence to:
Dr. Rex P. Hjelm
H805
Los Alamos National Laboratory
Los Alamos, NM 87545-1663
Tel: (505) 665-2372
FAX: (505) 665-2676
E-mail: Hjelm@lanl.gov

ABSTRACT

This is a study of the microstructure of particles of an experimental high surface area carbon black (HSA) and of the morphology of the particle aggregates using small-angle neutron scattering and the method of contrast variation. Contrast variation was effected by studying suspensions of the carbon black in cyclohexane containing different fractions of deutero-cyclohexane. We find that the approximately 29 nm diameter HSA particles are arranged as small, linear aggregates with average aggregation number between 4 and 6. The structure averaged over the particle population is best represented by a prolate ellipsoid of revolution with semi axes 14.5 and 76.4 nm. The surface of the aggregates appears smooth over length scales longer than 1 nm, which places an upper limit on the surface roughness observed by other methods. The internal structure of the aggregates is described by a shell-core model, with the shell density being consistent with a graphitic structure and the core being of lower density, more like amorphous carbon. Some fraction of the core volume (0.1 to 0.2) is taken up by voids that are not accessible to the solvent. An estimate of the shell thickness gives 1 to 2 nm along the ellipsoid minor axis and 6 to 10 nm along the major axis. The particles of the aggregate appear to be fused so that the less dense amorphous core is continuous through the inner parts of the aggregate. The information that can be obtained on the internal structure using contrast variation is limited by nonheterogeneity in the chemical composition of carbon black aggregates.

INTRODUCTION

Carbon black has numerous technical applications, including reinforcement of elastomers in durable rubber products, protection of plastics from degradation by ultraviolet radiation, and as a tint in ink and paints. It is not surprising that the microstructure and morphology of carbon black have been the focus of considerable effort by x-ray diffraction, electron microscopy and other techniques. [1] The considerable economic importance of this material makes it the subject of a substantial continuing research and development effort. The driving interest here is in understanding the structural role of carbon black in reinforcement of elastomers.

An understanding of the enhancement of useful mechanical properties of carbon black-rubber composites requires information on the structure of these materials on the scale of a few tenths to hundreds of nanometers and on making correlations of the structure with the mechanical properties of the materials. Information can be obtained on length scales below a few tenths of a nanometer using spectroscopic and gas adsorption techniques, and over length scales longer than around 4 nm using electron microscopic techniques. The intermediate length scales between 1

and 20 nm can be addressed with small-angle scattering methods but interpretations are difficult due to the complex nature of the composite structure over these length scales.

Difficulties in interpretation arise because fluctuations in scattering amplitude density, which give rise to scatter of radiation, can come from many sources some of which are not accounted for by the simplified models used in interpreting the data. Such complexities arise in a suspension of objects, say, from an inability to discriminate scattering from the shape and scattering arising from the internal structure. One way of sorting out the complexities of structure is to vary the scattering amplitude density of the solvent in the scattering experiment, the method of contrast variation. We outlined how this method might be employed in resolving the contributions of the two components in carbon black reinforced elastomers in an earlier communication. [2] Here we apply the method to the carbon black component, alone, embedded in cyclohexane. A preliminary report of this work was presented at the 143rd meeting of the American Chemical Society Rubber Division. [3]

The Method of Contrast Variation:

To review the method briefly: Suppose a population of objects suspended in a medium of scattering-length density, ρ_s , then the structure of each, $\rho(\mathbf{r})$, can be mathematically modeled as

$$\rho(\mathbf{r}) = \rho_s + (\bar{\rho}_p - \rho_s)\Omega(\mathbf{r}) + \zeta(\mathbf{r}) \qquad 1.$$

where $\rho(\mathbf{r})$ is the position-dependent scattering-length density, which is the structure of the solvent-excluding parts of the objects as seen by the neutrons. The shape of the solvent-excluding parts of the object is $\Omega(\mathbf{r})$, $\bar{\rho}_p$ is the average of $\rho(\mathbf{r})$ within the shape, and $\zeta(\mathbf{r})$, the internal structure function, is $\rho(\mathbf{r}) - \bar{\rho}_p$. The contrast is the difference between the average object scattering length-density and that of the solvent, $\Delta\rho = (\bar{\rho}_p - \rho_s)$.

The scattering intensity is proportional to the square of the scattering amplitude (the Fourier transform of equation [1]), and hence can be written as a quadratic in $\Delta\rho$. For a population of objects, as a function of momentum transfer, Q, the intensity is

$$I(\Delta\rho,Q) = \Delta\rho^2 I_{\Omega}(Q) + \Delta\rho I_{\Omega\zeta}(Q) + I_{\zeta}(Q) \qquad 2.$$

In this we assume that the population is chemically homogeneous and that the objects are uncorrelated in position and orientation. By chemically homogeneous we mean that all objects

have the same chemical composition and density. The momentum transfer is measured from the angle of scatter, 2θ, and the incident neutron wavelength, λ, as $Q = (4\pi/\lambda) \sin \theta$. The coefficients are $I_{\Omega}(Q)$, the scattering intensity due to the shape of the sample region that exclude solvent, and $I_{\zeta}(Q)$, the scattering intensity from the internal structure of the solvent-excluding part of the objects, and $I_{\Omega\zeta}(Q)$, which is the scattering due to the correlations between the shape and internal structure of the solvent-excluding part of the sample. There are important caveat to this analysis, which are discussed below, when the criterion of chemical homogeneity is not met.

The essential features of the method of contrast variation are that the solvent can be treated as a continuous medium in which the material of interested is embedded and that the contrast can be varied continuously. These conditions are easily met in solutions where the contrast can be varied by changing the fraction of deuterated to protonated solvent. Not all composites can be treated in this way, however, since there might not be a continuous phase, as there may be voids in the material, which contributes to the scattering and complicates interpretation. [4]

Implementation of the Method of Contrast Variation in Carbon Black and Composite Systems:

In the case of carbon black, reinforcement may be associated with the residual rubber remaining after extensive extraction of rubber-carbon black mixtures with a good solvent. This so called "bound rubber" with the carbon black can be dried, then swollen into a gel with a good solvent having different deuterated and protonated fractions. This affords the necessary change in ρ_s to vary the contrast against the interesting parts of the system. At the extremes one might imagine that the average scattering from one or the other component can be eliminated by matching the solvent. In practice, however, this applies only to the limit of zero scattering angle, as the fluctuations in scattering-length density within each component (corresponding to the third term in equation [2]) cannot be canceled and cannot in general be neglected.

This point was underscored in our previous measurements on the semi-reinforcing carbon black, N762, in deuterocyclohexane-cyclohexane mixtures. [2] With deuterated fraction, $f_d \cong 0.95$ (ρ_s near the contrast-match point) the scattering is characterized by a power law $I \sim Q^{-2.6}$. This result is consistent with plate-like geometry consistent with a graphitic component to particle structure. At other contrasts, away from the contrast match point, the scattering followed a considerably different power law dependence of $I \sim Q^{-3.6}$, characteristic of a polydisperse population of hard spheres. Such effects showed that there is very strong fluctuation in internal structure of carbon blacks, as represented in equation [1] by $\zeta(r)$.

The importance of this was confirmed by the observation in N762 composite gels with polyisoprene and SBR rubbers and in N121 composited with the same rubbers . Over a considerable part of the measured Q-domain, the scattering is dominated by carbon black. [2] Only at higher angles was scattering apparent from the polymer. This was determined from the changes that occurred in the scattering curves with contrast. The strong scattering due to the internal structure of the carbon black complicated further evaluation of the data.

The complexities of scattering from these systems point out that this approach on the structure of carbon black reinforcement requires a detailed study of the carbon black alone. The reasons for this are two fold. First we need a complete understanding of carbon black structure to serve as a comparison with the signal in the composite gels. Second, the internal structure of carbon black, which masked information from the polymer in the composite, must be determined to predict what information will be available on the polymer in measurements on the composite.

There are, of course, intrinsic aspects to the study of the carbon black by itself. The organization of carbon blacks is best described by a hierarchy of structures. [1] At the base level is the particle. These are not discrete entities in carbon black, but are covalently bound into aggregates. Aggregates further associate by Van der Waal's interactions to form agglomerates. Present notions on carbon black reinforcement of elastomers focus on the importance of particle size, aggregate geometry [5] and particle surface structure [6]. According to our present understanding highly branched aggregates may be more effective in producing the desired mechanical properties. SANS, by giving information on aggregate size and shape, provides a means for assessing this. SANS also provides information on surface roughness, and this also relates to assessing the effectiveness of carbon black processing in producing the desired characteristics. The comparisons between the carbon black alone and in the presence of elastomer may help determine what notions are relevant to an understanding of the composite properties. To this end we present a detailed study of an experimental high surface area carbon black, HSA, including a determination of the HSA aggregate form, aggregation number and internal structure.

There is a large literature in the use of small-angle scattering techniques in materials applications including studies aimed at understanding the structure of composite materials. [4,7,8] To our knowledge, this work and our previous communication [2] represent the first attempts to apply the method of contrast variation to a problem in materials science.

EXPERIMENTAL

Materials:

HSA carbon black was produced in an experimental single reactor pilot facility. The carbon black was collected with a water-cooled stainless steel probe. In this way the use of quench water was avoided, which would add contamination. The characteristics of HSA are listed in Table I.

Neutron Scattering:

Scattering measurements were done on the Low-Q diffractometer, LQD, at the Los Alamos Neutron Scattering Center, LANSCE. [9] The HSA carbon black was measured at 50 g/l in 0/100, 25/75, 50/50, 75/25 and 100/0 (v%/v%) deuterocyclohexane/cyclohexane. These mixtures are designated by the fraction C_6D_{12}, f_d. The sample was suspended by continuous rotation of the cell during the measurement. The cells had fused silica windows and the pathlength thorough the sample was 2.0 mm. Data acquisition and reduction were done as described elsewhere. [10-12] Scattering is reported as differential scattering cross section per unit mass, I(Q) (cm^2g^{-1}), as a function of momentum transfer, Q.

RESULTS

The solvent scattering length densities, ρ_s, of the different f_d are given in Table II. Also in Table II is the value of $\bar{\rho}_p$ calculated from the chemical compositions and densities of the carbon black in Table I. Thus we expect that the carbon black will be contrast matched by the solvent near $f_d \cong 0.92$.

The SANS from HSA at five different f_d are shown in Figs. 1 and 2. There is a strong dependence in both amplitude and shape of the curves on $\Delta\rho$. This is particularly noticeable in the $f_d = 1.0$ (Fig. 2b) and $f_d = 0.75$ curves (Fig. 2a). In the latter instance one sees a shoulder in the region $0.22 < Q < 0.44\ nm^{-1}$ (Fig 2a). The lines in Figs. 1 and 2 are for models discussed below.

Guinier Analysis:

The scattering from HSA (Figs. 1 and 2) is approximated at low Q by the Guinier approximation.

$$I(Q) = \Delta M_0 \exp\left(-\frac{1}{3}Q^2R_g^2\right) \qquad 3.$$

Here ΔM_0 is the contrast-weighted mass of the objects and R_g is the radius of gyration. The Guinier analysis implied by equation [3] is shown in Fig. 3, which is a plot of ln(I) verses Q^2. From this we extract ΔM_0 and R_g from the intercept and slope, respectively.

Analysis of the Contrast Dependence of the Guinier Parameters:

Equation [2] implies certain behavior for ΔM_0 with ρ_s that can be used to determine the contrast match point, $\bar{\rho}_p$. In our further analysis we assume that the objects referred to in equation [1] are aggregates of carbon black particles. Using the definition $\Delta M_0 = N_0/(nM)\ \Delta\rho^2 n^2 v_p^2$ (where n is the number of particles in the aggregate, v_p is the particle volume, M is the particle molecular weight and N_0 is the Avogadro constant), it follows that the contrast dependence of ΔM_0 should be

$$(\Delta M_0)^{1/2} = \left(\frac{N_0}{nM}\right)^{1/2} nv_p(\bar{\rho}_p - \rho_s) = \left(\frac{nv_p}{\rho}\right)^{1/2}(\bar{\rho}_p - \rho_s) \qquad 4.$$

where ρ is the density of the particle. Thus a plot of $(\Delta M_0)^{1/2}$ versus ρ_s, as given in Fig. 4 for HSA, should yield $\bar{\rho}_p$. The sign of the square root is chosen from prior knowledge of the approximate intercept shown in Table II, calculated from the chemical and density information in Table I. The slope should give nv_p, the aggregate volume, V_n. These considerations assume that all the aggregates have the same $\bar{\rho}_p$. If this is not so then the single contrast term in equation [4] must be replaced by a summation over all the aggregates. In this case the forward scattering will not go to zero, and the line for $(\Delta M_0)^{1/2}$ versus ρ_s will be discontinuous near $\bar{\rho}_p$. [13,14] Using data where equation [4] is still a good approximation will still yield the average value of $\bar{\rho}_p$. The data of Fig. 4 give a contrast match point, $\bar{\rho}_p = 5.7\ (0.3) \times 10^{10}\ cm^{-2}$ in good agreement with the value of $6.2 \times 10^{10}\ cm^{-2}$ calculated from the composition and density data (Table II). The slope is -5.3 (0.3) $\times 10^{-9}\ cm^3\ g^{-1/2}$, corresponding to aggregate volume $V_n = 5.4 \times 10^{-17}\ cm^3$ with the density from Table I.

Additional features of the aggregate structure can be obtained from the contrast dependence of R_g from the Guinier plots in Fig. 3. According to the formalism introduced by Ibel and Stuhrmann[15], the contrast-dependence of R_g is given by

$$R_g^2 = R_c^2 + \frac{\alpha}{\Delta\rho} - \frac{\beta}{\Delta\rho^2} \qquad 5.$$

In this, R_c^2 is the value of R_g^2 at infinite contrast, and thus includes contributions only from the aggregate shape. The second coefficient, α is approximated as the aggregate volume-normalized second moment of the internal structure scattering length density distribution, $\zeta(r)$, of equation [1]

$$\alpha \cong \frac{1}{V_n}\int_v \zeta(r) r^2 dv \qquad 6.$$

and β is related to the first moment of $\zeta(r)$, as

$$\beta = \left[\frac{1}{V_n}\int_v \zeta(r) r dv\right]^2 \qquad 7.$$

Values of R_g^2 plotted according to equation [5] are shown in Fig. 5. The data are consistent with a straight line ($\beta = 0$), implying a center of symmetry for $\zeta(\mathbf{r})$; if a curvature term were included it would give a non-physical negative value for β. This effect is probably due to chemical non homogeneity, as discussed below. We therefore use a straight-line fit to the data, which gives a very reasonable $\chi^2 = 3.0$ for 3 degrees of freedom. From this we obtain $R_c = 29.3$ (0.4) nm, and $\alpha = 2.0$ (0.3) x 10^{-2} . The value for α is large. That it is positive implies that the larger (positive) values of $\zeta(r)$ are concentrated toward the outer part of the spherically-averaged structure. The value for R_c suggests a radius of 37.8 nm, assuming spherical aggregate shape, giving an aggregate volume, V_n, of 2.3 x 10^{-16} cm^3, far larger than the value determined from the slope in Fig. 4. This discrepancy suggests non-spherical aggregate shape, as discussed below. The values of R_c and α are not greatly affected by possible chemical non homogeneity. [13] This is discussed further below.

Basic Scattering Functions:

The three basic scattering functions derived by fitting the contrast dependence of the scattering to equation [2], using the experimentally determined contrast match point, are shown in Figs. 6 and 7.

The first term, I_Ω, (Fig. 6) is very useful in giving information on the contribution of the scattering intensity from the shape of the aggregate independent of the contribution of internal structure. It is determined by extrapolation to infinite contrast; thus, it is not sensitive to a choice of $\bar{\rho}_p$, and it is not affected by the presence of non homogeneity in chemical composition and density Simple consideration of this function allows calculations of aggregate size, shape and volume.

The intercept of the Guinier plot of $I_\Omega(Q)$ gives $I_\Omega(0) = 2.4\ (0.1) \times 10^{-17}$ cm^6/g. From equations [2-4], $I_\Omega(0)$ must equal the volume-squared on the per gram scale (cm^6/g). The volume per aggregate calculated by multiplying $I_\Omega(0)$ by the density in Table I is $V_n = 4.6 \times 10^{-17}$ cm^3. From the Guinier analysis $R_c = 34.1\ (0.9)$ nm, about 15% larger than the value of R_c calculated from the Stuhrmann analysis in Fig. 5; in theory these should be equal because the "infinite-contrast" scattering is dominated by the I_Ω term.

A significant feature of the shape-internal structure cross term function, $I_{\Omega\zeta}$, shown in Fig. 7a is the negative values observed for Q below 0.3 nm^{-1}. This feature reflects the characteristic of the internal structure in which material of higher scattering length density surrounds material of lower scattering length density. The positive value of α is due to this feature of $I_{\Omega\zeta}$. It is anticipated that $I_{\Omega\zeta} \rightarrow 0$ as $Q \rightarrow 0$. Although the statistical uncertainties from the least-squares extraction of this term become large at low Q, the data at low Q do not go to zero. This is probably due to non homogeneity of the aggregates, though we will see below that this is an important consideration for only the low Q portion of this function.

Interpretation of the internal structure function (Fig. 7b) is more problematic due to the strong influence of non homogeneity, particularly at low Q where the function does not have the expected behavior and vanish as $Q \rightarrow 0$. The region above 0.2 nm^{-1} does fit the scattering expected from a shell like structure (see below).

Aggregate Shape:

The shape of $I_\Omega(Q)$ over lower Q values is consistent with an elongated shape having an aspect ratio, $\gamma \cong 5.3$. This is seen by fitting the curve to the scattering expected from a prolate ellipsoid of revolution [16]

$$I(Q) = 9\int_0^{\pi/2} \left\{ \frac{a_o^3 \gamma_o [\sin\beta(\theta) - \beta(\theta)\cos\beta(\theta)]}{\beta(\theta)^3} \right\}^2 \cos\theta \, d\theta \qquad 8a.$$

with

$$\beta(\theta) = Qa(\cos^2\theta + \gamma^2 \sin^2\theta)^{1/2} \qquad 8b.$$

The fit of $I_\Omega(Q)$ gives semi-axes a ≅ 14.5 nm and b≅ 76.4 nm (γ = 5.3, R_c = 34.1 nm). The scattering expected for this model is shown in Fig. 6 for comparison with I_Ω. The excellent fit of the model with the data at low Q values is strong evidence for the elongated shape of the aggregate. The deviation of the model from the data in the mid-Q range is probably a consequence of polydispersity in aggregate shape, which has not been included in the model. The total volume of this fitted ellipsoid of revolution is $V_n = 6.7 \times 10^{-17}$ cm^3. This is somewhat larger than the estimates calculated from the measured density (Table I), suggesting that the real aggregate density is somewhat higher than the measured density.

Electron microscopy reveals that carbon black aggregates are made up of more or less identical spherical carbon black particles. [1] Our observations of HSA aggregates by transmission electron microscopy (TEM) confirm this. TEM results also show the HSA particles to be 27 (7) nm in diameter. The TEM result is consistent with the ellipsoid minor axis diameter of 24 to 29 nm determined by the SANS measurements. This along with the shape information from I_Ω leads to the proposal that the HSA aggregates suspended in cyclohexane are a linear arrangement of HSA particles. The average number of HSA particles in the aggregate, n, from the aspect ratio, γ, is 5-6. From the diameter of the HSA particles their volume must be in the range 0.7 to 1.2 x 10^{-17} cm^3. Comparison of these values of v_p with V_n for the aggregate also gives n in the range 5-6.

Surface Roughness of the Aggregate:

One additional conclusion that can be drawn from the shape scattering function in Fig. 6 is that the HSA particles are smooth on length scales from 5 to 1 nm. This is determined from the Porod Law ($I \sim Q^{-4}$) scattering for $0.2 \geq Q \geq 1.0$ nm^{-1} (Fig. 6). allowing for the incoherent scattering . A rough surface on these length scales would have had a weaker power law dependence. That the black particles are smooth is consistent with our earlier observation on N762. [2] There the scattering showing a power law $I \sim Q^{-3.6}$, which was interpreted as scattering from a polydispersed population of smooth sphere-like particles. It is not possible to infer surface structure from $I_\Omega(Q)$ at larger Q (hence smaller length scales) owing to the crossover to incoherent scattering for $Q \geq 1$ nm^{-1} (Fig. 5), which obscures any further information. The shape and volume calculations given above suggest that the surface area on length scales down to 1 nm is at most 1.0 to 1.3 x 10^6 cm^2/g. This is considerably less than the surface area determined from nitrogen adsorption (Table I), suggesting that the roughness implied by gas absorption

measurements is on length scales much smaller than that accessible by SANS. The work of Zerda and colleagues [6] suggests that carbon blacks have a surface fractal dimension of 2.2 over length scales of 0.1 to 0.2 nm. The results from SANS show that the upper limit on this feature is approximately 1 nm. Roughness may relate to the area available to binding rubber, and these results in comparison with surface area obtained by other techniques, probing small length scales (Table I), show the limit to the scale of the roughness in HSA particles.

The Aggregate as a Linear Array of Spherical Particles:

The prolate ellipsoid of revolution derived from I_Ω should be considered as an "average" structure that reflects the elongated structure of the aggregates. We consider further information available from the analysis of the radius of gyration assuming that the aggregate is a linear array of spherical particles, like beads on a string.

We require an expression for the contrast dependence of the radius of gyration for an array of identical particles. Such an expression is obtained be using the derivation of Ibel and Stuhrmann [15] and applying a theorem for adding second moments. The result is an equation analogous to [5] for any aggregate of identical particles,

$$R_g^2 = R_{cp}^2 + \overline{r^2} + \frac{\alpha_p}{\Delta\rho} - \frac{\beta_p}{\Delta\rho^2} \qquad 9$$

where the quantities identified with the subscript, p, refer to the individual particles in the aggregate. By equating like powers in $\Delta\rho^{-1}$ in equations [5] and[9] we see that R_c in equation [5] can be equated with the first two terms of equation [9], and shows the contribution to R_c from the average of the second moment of the distribution of particles in the array $\overline{r^2}$. The contrast-dependent parts, α_p and β_p, reflect only single particle internal structure, independent of the details of how they are arranged in the aggregate. We consider the implication of the contrast-independent and contrast-dependent parts separately.

Starting with the contrast-independent part of equation [9] (the first two terms), we calculate $\overline{r^2}$ in equation [9] for a linear array. The resulting equation is rearranged to give an expression for the aggregation number,

$$n = \left[3\frac{R_c^2 - \frac{3}{5}R_o^2}{R^2} + 1 \right]^{\frac{1}{2}} \qquad 10$$

where the particle radius is, $R_o = \sqrt{\frac{5}{3}} R_{cp}$. Solving this relation for n with R_c equal to 29.3 to 34.1 nm for R_o from 12 to 14.5 nm, consistent with the SANS and TEM results above, give the aggregation number in the range n = 4.1 to 4.8. These calculations along with the considerations given above bracket the range of values for n in the interval 4 to 6.

Shell-Core Spherical Particles:

TEM [1] and scanning tunneling microscopy (STM) [17,18] measurements of carbon blacks suggest that carbon black particles have a shell-core structure, consisting of a layer of ordered zones of graphitic crystallites around an amorphous core, which includes some voids. The value for α lends some light on the model derived from the microscopy studies.

We derive an expression for α for a concentric shell-core model, either spherical or confocal ellipsoid of revolution, using the relationship in equation [6] and doing the integration in prolate spheroid coordinates. The result is,

$$\alpha = (\rho_o - \bar{\rho}_p)(R_c^2 - R_i^2) \qquad 11$$

where ρ_o is the scattering-length density in the outer shell, and R_i^2 is the squared radius of gyration of internal region of the particle. In deriving expression [11] we used the definition of the internal structure function, which requires that $\int_v \zeta(r)dv = 0$. The problem then reduces to solving for R_i^2 , in equation [11], as a function of ρ_o, given α, R_c and $\bar{\rho}_p$. For the case of an array of spherical particles $\alpha = \alpha_p$ of equation [9], but since we do not have a direct measurement for $R_c = R_{cp}$ we must use the range of values consistent with the particle radius from TEM, R_c and I_Ω, namely 12 to 14.5 nm. We specify a range of values for ρ_o from the known range of densities and chemical compositions of carbon blacks, specifically acetylene black ($C_{600}H_{60}$, ρ = 1.87 g/cm^3), pyrolytic carbon (ρ = 2.06 g/cm^3), and graphite (ρ = 2.27 g/cm^3). [21]

Inspection shows that there are no real solutions given the range of acceptable particle R_{cp}, ρ_o and ρ_i values consistent with the measured value of α_p. A particle radius of at least 18 nm must be

assumed to account for the observed α value. This radius is significantly outside the range of sizes determined by TEM for HSA and from the SANS shape analysis.

An Elliptical Shell-core Model:

An alternative to the beads on a string model is that the particles observed by TEM are fused together in the aggregate so that the less dense core material is continuous through the aggregate. We go back to the "average" structure represented by the prolate ellipsoid of revolution derived above, but now allow that its contrast-dependence is determined by an overall shell-like structure. We could consider the solutions for to equation [11], however, this model places too much scattering mass along the minor axis of the ellipsoid to account for the value of α derived from Fig. 5. Instead we consider an alternative model (among many), for which equation [11] is a reasonable approximation, in which the shell and the core have the same aspect ratio (rather than being confocal). This the model has a continuously changing shell thickness with the thicker (Δt_{max}) part being along the major ellipsoid axis and the thinner part (Δt_{min}) being along the minor axis. This mathematical convenience has the advantage of giving a representation the uncertainties in the calculation of the shell thickness. Thus we can treat Δt_{max} and Δt_{min} and the density of the inner core, ρ_i as model parameters to be adjusted to agree with the analyses in Figs 4 and 5. The two values of R_c (Figs. 5 and 6) are used as examples of the range of values consistent with the data, and results are computed as a function of the shell density, ρ_o.

The results (Fig. 8) show that The average density of the core is not sensitive to the choice of ρ_o,in the range between graphite and pyrolytic carbon or R_c. In this domain ρ_i has values from 1.75 to 1.77 g/cm^3. These densities imply that the fraction of the core volume that is void, inaccessible to solvent is between 0.10 and 0.22, depending on the assumption made for the structure of the carbon in the inner core. The results also place limits on the shell thickness. The minimum shell thickness along the major semi axis is 3.6 nm and 0.8 nm along the minor axis. The shell thickness span a range from 2 to 10 nm if the shell density is assumed to be more like pyrolytic graphite (Fig. 8). If we assume that ρ_o is less than that for pyrolytic graphite the shell thickness must be increased, and ρ_i decreased considerably (to the point where the core must be almost entirely void) in order to be consistent with the analyses in Figs. 4 and 5.

Therefore the estimate for α is only consistent with a model where the spherical particles in the aggregate fuse together so that the less dense cores are continuous through the structure, and there is no partitioning of the particle cores by more dense shell material. This conclusion is in disagreement with the recent hypothesis of Donnet *et al* [17] that the particles are tangent to one

another with at least a few interpenetrating crystallite layers partitioning the particles in the aggregate. Again, the ellipsoidal shell model must be considered as an average structure of a polydisperse population of aggregates.

Contrast-dependent Scattering of an Elliptical Shell-core Particle:

With some idea of the structure of the aggregates and particles we consider whether the detailed models can represent all the data shown in Figs. 1 and 2. We calculate the contrast-dependent scattering for the concentric shell ellipsoid model by modifying equation [8] to give

$$\frac{d\sigma}{d\Omega}(Q) = 9\int_0^{\pi/2}\left\{\frac{(\rho_o-\rho_s)\,a_o^3\gamma_o[\sin\beta_o(\theta)-\beta_o(\theta)\cos\beta_o(\theta)]}{\beta_o(\theta)^3} - \frac{(\rho_o-\rho_i)\,a_i^3\gamma_i[\sin\beta_i(\theta)-\beta_i(\theta)\cos\beta_i(\theta)]}{\beta_i(\theta)^3}\right\}^2\cos\theta\,d\theta \qquad 12.$$

which is average differential cross section (cm^2) per particle. Here β_i and β_o, correspond to the analogous quantity in equation [8], but apply to the core and shell parts of the aggregate, respectively. The calculation is scaled by 6×10^{15} to match the data, which is normalized on the gram scale, implying $\approx 2 \times 10^{-16}$ g/particle. Effects of instrument resolution and polydispersity, both of which smear the calculated curve, are not taken into account. The results, shown in Fig. 1 and 2 as solid lines compared with the data, show that the model gives a good reproduction of the contrast dependence of the low-Q scattering, with the exception of the sample at $f_d \cong 0.75$, where at the lowest Q values the data are as much as twice as intense as the calculation. This is due to chemical polydispersity. Particles of composition different from the average make significant contributions to the total scattering near $\bar{\rho}_p$. It is notable, however, in this sample that the shoulder at $\cong 0.2$ nm^{-1} is well reproduced by the simulation, indicating that this particular feature is due in part to the particle internal structure, as seen from the simulation of the scattering expected from a calculation for $I\zeta$, the scattering expected for the contrast match point of a chemically homogeneous population of shell-core ellipsoids (Fig. 2a). We note too that this calculated value for $I\zeta$ fits the experimentally determined function well for Q greater than 0.2 nm^{-1} (Fig. 7b).

Scattering from a Linear Array of Spherical Shell-core Particles:

As we discuss below, polydispersity can have an effect on the determination of α. Therefore, we explore the effects of different α on our conclusion. We considered solutions for the structure of

spheroidal particles in the R_o domain 12 to 14.5 nm. If α is about 1/3 of the values determined here, then real solutions for ρ_i and R_i are found, but the value of ρ_i is very small. Consequently, the carbon in the core would have to be largely void. We can also do a calculation for the scattering expected for a linear array of such particles. Because the particles are approximately spherical the total scattering intensity for a single aggregate can be approximated by

$$\frac{d\sigma(Q)}{d\Omega} = F^2(Q)\, S(Q) \qquad 13.$$

where S(Q) is the structure factor describing the scattering due to the arrangement of the spheres in the aggregate. The structure factor is given by

$$S(Q) = \frac{1}{n}\sum_{j=1}^{n}\sum_{k=1}^{n}\frac{\sin Qr_{jk}}{Qr_{jk}}$$
$$= \frac{1}{n}\left[1 + 2\sum_{j=1}^{n}(n-j)\frac{\sin jQR_o}{jQR_o}\right] \qquad 14.$$

for a linear array. $F^2(Q)$ is the form factor of the spherical shell-core particles given by equation [12] with $a_o = R_o$, $a_i = R_i$, $\beta_o = QR_o$ and $\beta_i = QR_i$, when $\gamma = 1.0$. We anticipate that the number of particles in an aggregate will be given by some probability density function P_n, which we take to be Poisson. This gives an effective structure factor $S_{eff}(Q) = \Sigma_n P_n S_n(Q)$. We use the mean value $\mu_n = 4.5$ calculated above. The results show (dashed lines in Figs 1 and 2) that the calculated scattering curves for this model do not fit the data. The very strong fluctuations in scattering length density along the major axis of the aggregate introduced by the spherical shells lead to much higher scattering at larger Q than actually observed. This becomes progressively apparent as the contrast is reduced, to the point where the observed scattering for $Q > 0.1$ is five times smaller than the calculated value. This is particularly apparent when the contrast of the core and shell are reversed in 100% d-cyclohexane, here features are apparent that are not seen in the data that come from the internal structure of the particles. These result further argue against simple association of shell-core like spherical particles so that the less dense cores are interspersed by denser material. In principal, if the difference between the core and shell densities were reduced sufficiently, the differences between the observed and calculated scattering would be reduced accordingly, but this would require a reduction in the value of α by more than an order of magnitude from that observed here.

DISCUSSION

The Method of Contrast Variation:

The method of contrast variation allows separation of contributions from internal structure and object shape to the scattering. As a consequence more information has been obtained on the particle microstructure and morphology than previously available from scattering measurements. There are important caveats. Equation [2] implies that scattering must have a parabolic dependence on contrast but strictly speaking this can be so only if the coefficients in [2] are independent of the contrast. Chemically homogeneity is required for this condition to be met. Deviation from the predicted behavior near the contrast match points are evidence that the aggregates are not chemically homogeneous. Consequently, the quantities in equations [2] and [5] must be replaced by sums over objects with different chemical composition. We explore briefly the effects of this on our interpretation of the analysis.

The parameters R_c and I_Ω, in equations [2] and [5] are not sensitive to non homogeneous chemical composition, as they are determined by extrapolation to infinite $\Delta\rho$. On the other hand non homogeneity has considerable effect on I_ζ and $I_{\Omega\zeta}$, as illustrated in Figure 7, which shows that both functions are significantly affected at low Q. This is anticipated, as the shape contributions from particles that are not contrast matched at $\bar{\rho}_p$ are going to become more significant as Q becomes smaller. This effect evidently becomes less important at larger Q, where the scattering functions are fitted well by the model scattering law calculated for the core shell ellipse model in Fig. 7b above Q = 0.2 nm^{-1} for I_ζ, and above 0.07 nm^{-1} for $I_{\Omega\zeta}$ (Fig. 7a). The parameter α is also affected by non homogeneity. How this affects the determination of α is seen by considering what happens to the apparent R_g as the contrast is changed. At large $\Delta\rho$, chemical non homogeneity has little effect. At small $\Delta\rho$, however, the radius of gyration from objects not well contrast matched dominates the measured R_g, resulting in a higher value for R_g than anticipated. Thus the magnitude of α will not be changed to any large extent, as pointed out in earlier work by Stuhrmann et al. [13] This effect is a likely explanation for the, unphysical curvature of the Struhman analysis in Fig. 5.

Carbon Black Microstructure and Morphology:

The organization of carbon blacks is best described as a hierarchy of structures. At the base level is the particle. Particles are covalently bound into aggregates, and aggregates form agglomerates held together by Van der Waal's forces. Particle surface roughness and size, as well has aggregate morphology are thought to contribute to the reinforcing properties of carbon black. This work on

suspensions of HSA carbon black in cyclohexane gives further information on the structures of the particles and aggregates.

Electron microscopy studies show an apparent structure for the aggregates that can be classified into a variety of shape types. [1] These include round, ellipsoidal, linear and branched. It has been proposed that the geometric dimensionality of the aggregates could be related to the reinforcement of elastomers by carbon blacks. [1,5] This view has been called into question by a recent stereoscopic electron microscopy study of highly dispersed carbon blacks which indicates that aggregates of N220 and N660 are largely linear structures. [19,20] The SANS results are consistent with this latter view, as we find largely one-dimensional association (a linear array) of the carbon black when suspended in cyclohexane and that the average aggregation number is quite small, $n \approx 4$-6. However, it is not possible to rule out small amounts of branching on length scales up to 50 nm. If this result can be generalized to other reinforcing blacks, then the association of aggregate branching with reinforcing may be called into question.

Estimates of the size of carbon black aggregates range from about 5 to 100. [1] In some older examples in the literature where the samples are not well dispersed this number has been estimated as several hundred. Certainly, our estimate of $n \approx 4$ to 6 is well below the size usually estimated from electron microscopy. The discrepancy could be the result of agglomerate association on the carbon foils. The observations of stereo TEM measurements [19,20], support smaller aggregation numbers for N220 and N660, but not as small as those observed here. With regard to the TEM observations on aggregation and form, there are issues of the effectiveness of dispersion and on interactions of the aggregates with the carbon foils used to support the samples.

Models derived from high resolution microscopy techniques show the particle to be a spheroidal core-shell structure. [1,17,18] The shell is proposed to consist of graphitic crystallites interspersed with less ordered carbon regions [17,18] with concentric ordering of plate-like structures in the shell. [1] The graphitic layers are parallel to the particle surface. [1] The surface of the carbon black particles contain pores [1], and overall the particle surface is rough according to gas adsorption studies. [6] The core is composed of less dense amorphous carbon. [1] Other work indicates that the core includes voids, which may or may not be connected to the exterior. [1]

The SANS results are consistent with the shell-core morphology, but the large value of α is not consistent with the particles being bound by the graphite-like shells. Rather, the SANS results indicate that the dense material does not penetrate into the core of the aggregate, but confined more or less to the outer part of the aggregate. This picture, shown in Fig. 9, is one where the particles make up the aggregate so that the less dense cores are fused together to make the void-

containing core continuous throughout the interior of the aggregate. We must allow that there can be systematic error in the relatively large value of α computed here from the contrast dependence of the low-Q scattering due to the compositional polydispersity (see above). We find that the value of α would have to be at least an order of magnitude smaller than that observed here to be consistent with interspersion of the graphite like material into the center of the aggregates, as envisioned by the hypothesis of Donnet et al. [17] Such a large error in our determination seems unlikely, given the considerations above. Further, the forms of the scattering curves at low contrast argue further against such interpenetration of highly dense material into the core of the aggregate. Our results suggest that the particles fuse so that the amorphous cores become a single entity throughout the center of the aggregate structure.

The range of thickness of the dense shell was considered with the aid of equation [11], and shown to be of the order 1 to 2 nm at the thinnest 4-10 nm at the thickest, depending on the density chosen for the shell material (Fig 8). The range of plausible outer shell densities is consistent with high resolution TEM observations. [1] We reaches a similar conclusion in our earlier measurements on N762 were we observed the presence of sheetlike structures near the contrast match point, suggesting graphitic internal structure. [2]

This information on carbon black aggregate form and an internal structure can be used with like measurements made on carbon black-elastomer composites to obtain information on the structures and aggregation of each component. A comparison of the signals will give important information on the aggregation of carbon black particles in bound rubbers.

CONCLUSIONS

The structure of high surface area (HSA) carbon black as a suspension in cyclohexane has been studied in detail using small-angle neutron scattering (SANS) and the method of contrast variation. The results of this study offer a refinement of models derived from other methods of physical characterization. The particles of this carbon black form small, linear aggregates with average aggregation number in the range 4-6. This value is at the lower range of estimates of aggregation number given by previous electron microscopic investigations. The overall size and shape of the aggregates is best described by an elongated structure that can be represented by a prolate ellipsoid of revolution with semi-axes in the range 12-14.5 and 60-76.4 nm. The aggregates show a shell-core-like structure. The outer shell consists of graphite-like material and is between 6 and 10 nm at its thickest. The less dense core of amorphous carbon is continuous through the center of the aggregate. The surface of the aggregate is smooth over the length scales probed by SANS, suggesting an upper limit to the roughness observed by gas

absorption techniques of about 0.2 nm. Compositional polydispersity plays a role in the information that is available from this system using the method of contrast variation.

ACKNOWLEDGMENTS

This work was supported by a grant from the Office of Basic Energy Sciences of the Department of Energy. This work benefited from the use of the Low-Q Diffractometer at the Los Alamos Neutron Scattering Center of the Los Alamos National Laboratory which is supported by the Office of Basic Energy Sciences of the United States Department of Energy under contract W-7405-ENG-36 to the University of California.

REFERENCES

1. Hess, W.M. and Hurd, C.R., "Microstructure, Morphology and General Physical Properties" in *Carbon Black*, J.-B. Donnet, R.C. Bansal, and M.-J. Wang, eds., Dekker, New York, pp 91-106 (1993), and references there in.
2. Hjelm, R.P., Wampler, W., and Seeger, P.A. "Microstructure of Composite Materials Using Small-angle Neutron Scattering and Contrast Variation: Approaches Toward Understanding the Structure of Carbon Black Elastomer Mixtures", *Polymers & Polymer Composites*, 1, 53A-70A, (1993).
3. Hjelm, R.P., Wampler, W., and Seeger, P.A. "Small-Angle Scattering, Contrast Variation and the Study of Complex Composite Materials." *Proceedings of the 143rd Meeting of the American Chemical Society Rubber Division*, Denver, 1993, Rubber Division, ACS, Akron, OH paper 32.
4. Wignall, G.D., Farrar, N.R., and Morris, S., "Characterization of Carbon-filled Polymers by Small-angle Scattering Techniques", *J. Mater. Sci.* , **25**, 69-75 (1990).
5. Gerspacher, M, and O'Farrell, C.P., "Carbon Black as a Fractal Object: An Advanced Look at an Important Filler", *Elastomerics*, **123** (4), 35-39 (1991).
6. Zerda, T.W., Yang, H., and Gerspacher, M., "The Fractal Dimension of Carbon Black Particles", *Rubber Chem. & Tech.*, **65**, 130-138 (1992).
7. Wu, W.-l., "Small-angle X-ray Study of Particulate Reinforced Composites", *Polymer*, **23**, 1907-1912 (1982).
8. Young, R.J., Al-Khudhairy, D.H.A., and Thomas, A.G., "Characterization of Filled Rubber Using Small-angle X-ray Scattering", *J. Mater. Sci.*, **21**, 1211-1218 (1986).
9. Seeger, P., Hjelm, R.P. and Nutter, M, "The Low-Q Diffractometer at the Los Alamos Neutron Scattering Center", *Mol. Cryst. Liq. Cryst.*, **180A**, 101-117 (1990).
10. Hjelm, R.P., "Resolution of Time-of-Flight Low-Q Diffractometers: Instrumental, Data Acquisition and Reduction Factors", *J. Appl. Cryst.*, **21**, 618-628 (1988).

11. Hjelm, R.P., and Seeger, P.A., "Time-of-Flight Small-angle Neutron Scattering Data Reduction and Analysis at LANSCE with Program SMR", *Conferences in Physics*, **97**, 367-387 (1989).
12. Seeger, P.A., and Hjelm, R.P. "Small-angle Neutron Scattering at Pulsed Spallation Sources", *J. Appl. Cryst.*, **24**, 467-478 (1991).
13. Stuhrmann, H.B. and Duee, E.D., "The Determination of the Scattering Density Distribution of Polydispersed Solutions by Contrast Variation: a Neutron Scattering Study of Ferritin", *J. Appl. Cryst.*, **8**, 538-542 (1975).
14. Stuhrmann, H.B., Haas, J., Ibel, K., Koch, M.H.J., and Crichton, R.R., "Low Angle Neutron Scattering of Ferritin Studied by Contrast Variation", *J. Mol. Biol.*, **100**, 399-413 (1976).
15. Ibel, K., and Stuhrmann, H.B., "Comparison of Neutron and X-ray Scattering of Dilute Myoglobin Solutions", *J. Mol. Biol.*, **93**, 255-265 (1975).
16. Guinier, M.A., "La Diffraction des Rayons X aux Très Petits Angles: Application a L'Étude de Phénonènes Ultramicroscopiques", *Ann. de Phys.*, **12**: 161-237, (1939).
17. Donnet, J.-B. and Custodéro, E., "Carbon Black Surface Studied by Scanning Tunneling Microscopy", in *Carbon Black*, J.-B. Donnet, R.C. Bansal, and M.-J. Wang, eds., Dekker, New York, pp 221-227 (1993).
18. Donnet, J.B., and Custodéro, E., "Ordered Structures Observed by Scanning Tunneling Microscopy at Atomic Scale on Carbon Black Surfaces", *Carbon*, **30**, 813-815 (1992)
19. Gruber, T.C., Zerda, T.W., and Gerspacher, "Three Dimensional Morphology of Carbon Black Aggregates", *Carbon*, **31**, 1209-1210.
20. Gruber, T.C., Zerda, T.W., and Gerspacher, "3 D Morphological Characterization of Carbon Black Aggregates Using Transmission Electron Microscopy", *ACS Rubber Division, 144th Meeting, October 26-29*, paper No. 164 (1993).
21. Kinoshita, K. *Carbon: Electrical and Physicochemical Properties*, J Wiley, New York, pp 12 (1988).

FIGURE LEGENDS

Figure 1. *Contrast-Dependent Scattering from HSA:* A slurry of a high surface area carbon black, HSA in different mixtures of deutero-cyclohexane/cyclohexane. O, data; ———, calculated scattering from the ellipsoid model described in the text; -----, calculated scattering from the linear array of spheres model described in the text. A, f_d= 0; B, f_d= 0.25; C , f_d = 0.50.

Figure 2. *Contrast-Dependent Scattering from HSA (Continued):* A slurry of a high surface area carbon black, HSA in different mixtures of deutero-cyclohexane/cyclohexane. O, data; ———, calculated scattering from the ellipsoid model described in the text; -----, calculated scattering from the linear array of spheres model described in the text. A, f_d= 0.75, ———, scattering calculated for the ellipsoid model described in the text, but at f_d= 0.86 ; B, f_d= 1.0.

Figure 3. *Guinier Analysis of Scattering from HSA:* Low-Q data from Figs. 1 and 2 plotted according to equation [3]. O, f_d = 1.0; ●, f_d = 0.75; □ f_d = 0.50; ■, f_d = 0.25; ◇, f_d = 0. ———, fit to the data by equation [3].

Figure 4. *Plot of $[\Delta M_0]^{1/2}$ verses Solvent Scattering-length Density, ρ_s :* I(Q) fit to the Guinier approximation (equation [3], in Fig. 3) and extrapolated to Q = 0 to give ΔM_0. This is then plotted according to equation [4], O. ———, Regression according to equation [4].

Figure 5. *Plot of the Radius of Gyration Squared verses the Inverse of the Contrast:* Data plotted according to the analysis implied by equation [5]. Line is the fit to equation [5] with $\beta = 0$.

Figure 6. *Shape Scattering Function, $I_\Omega(Q)$:* O, values calculated by fitting equation [2] to the data in Figs. 1 and 2 for each Q. Solid curve is scattering intensity expected from an ellipsoid, as described in the text. Solid line illustrates a Porod law, $I \sim Q^{-4}$.

Figure 7. *Cross Term Scattering Function, $I_{\Omega\zeta}(Q)$ and the Internal Structure Scattering Function $I_\zeta(Q)$:* A, $I_{\Omega\zeta}(Q)$; B. $I_\zeta(Q)$. O, values calculated by fitting equation

[2] to the data in Figs. 1 and 2 for each Q. ——— , expected for the shell-core ellipsoid model as explained in the text.

Figure 8. *Calculation of Shell Thickness and Core Density for an Ellipsoid Shell Core Model:* Solutions for equation [11] for the core density, ρ_i, and shell thickness along the major axis, Δt_{max}, and the minor axis, Δt_{min}, as a function of outer shell density, ρ_o. Values for α and $\bar{\rho}_p$ are given in the text. Lines are solutions using, ———, R_c = 34.1 nm, and — — — , R_c = 29.3 nm. The arrows at A and B mark, respectively, the densities of graphite and pyrolytic carbon.

Figure 9. *Cartoon of the Carbon Black Aggregate Structure:* A representative structure derived from SANS and high resolution microscopy of a typical HSA carbon black aggregate consisting of a linear array of spheroidal particles. The average aggregation number is 4 to 6 with particle sizes being in the range of 24 to 29 nm. The outer shell of the structure (black) consists of graphitic carbon crystallites, with a core (gray) of less dense void-filled (white) carbon. The less dense core is contiguous throughout the aggregate.

Table I

Characteristics of HSA Carbon Black used in this Study

DBP (cm^3/g)	1.508
24M4 DBP (cm^3/g)	1.057
N_2 surface area (cm^2/g)	1.876×10^6
Transmitance (%)	98
Tent Strength	136.0
Density (g/cm^3)	1.91

Chemical Composition (weight %)

C	H	O	S
97.33	0.19	0.78	1.70

Table II

Average Scattering Length Densities

C_6D_{12}/C_6H_{12} Mixtures		HSA	
f_d	ρ_s (10^{10} cm^{-2})	f_d	$\bar{\rho}_p$ (10^{10} cm^2)
0	-0.28	0.92	6.17 [a]
0.25	1.46	0.86	5.7 (3) [b]
0.50	3.20		
0.75	4.94		
1.00	6.68		

a An estimate of the average neutron scattering length densities, $\bar{\rho}_p$, for the carbon black and elastomer components were calculated from the density, ρ, and elemental analysis as, $\bar{\rho}_p = \rho N_0 \Sigma b_i w_i / m_i$. Here, b_i is the neutron scattering length and m_i is the gram atomic weight. w_i is the mass fraction of element i from the elemental analysis in Table I.

b Determined from the $\sqrt{I(0)}$ verses ρ_s plot shown in Fig . 4 and calculated as described in the text.

Fig 1

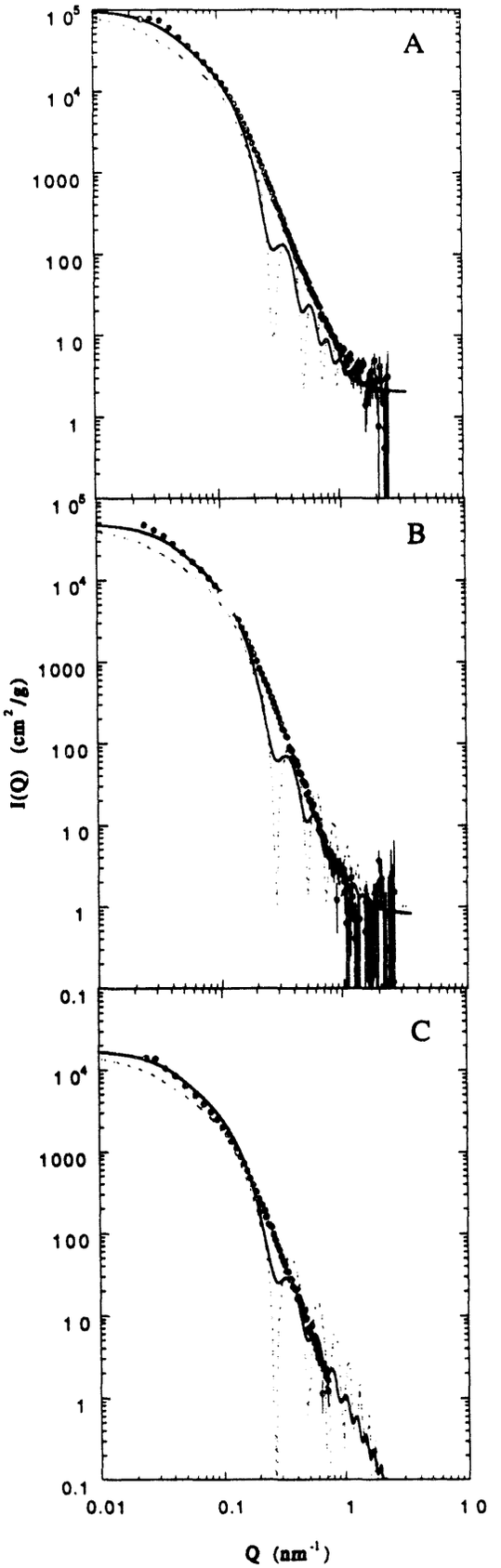

Fig 2

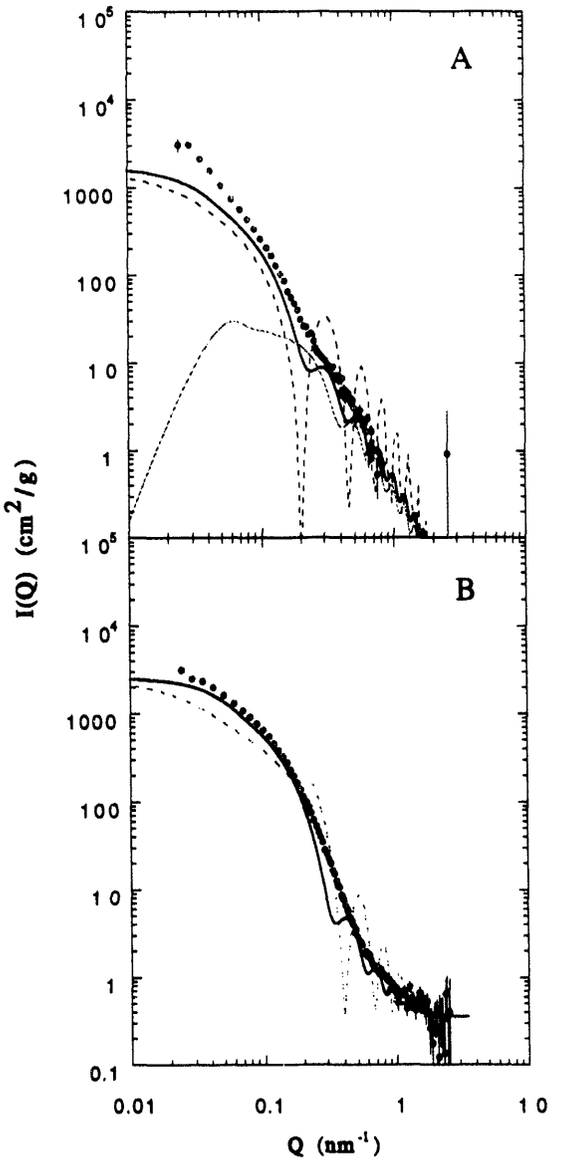

Fig 3

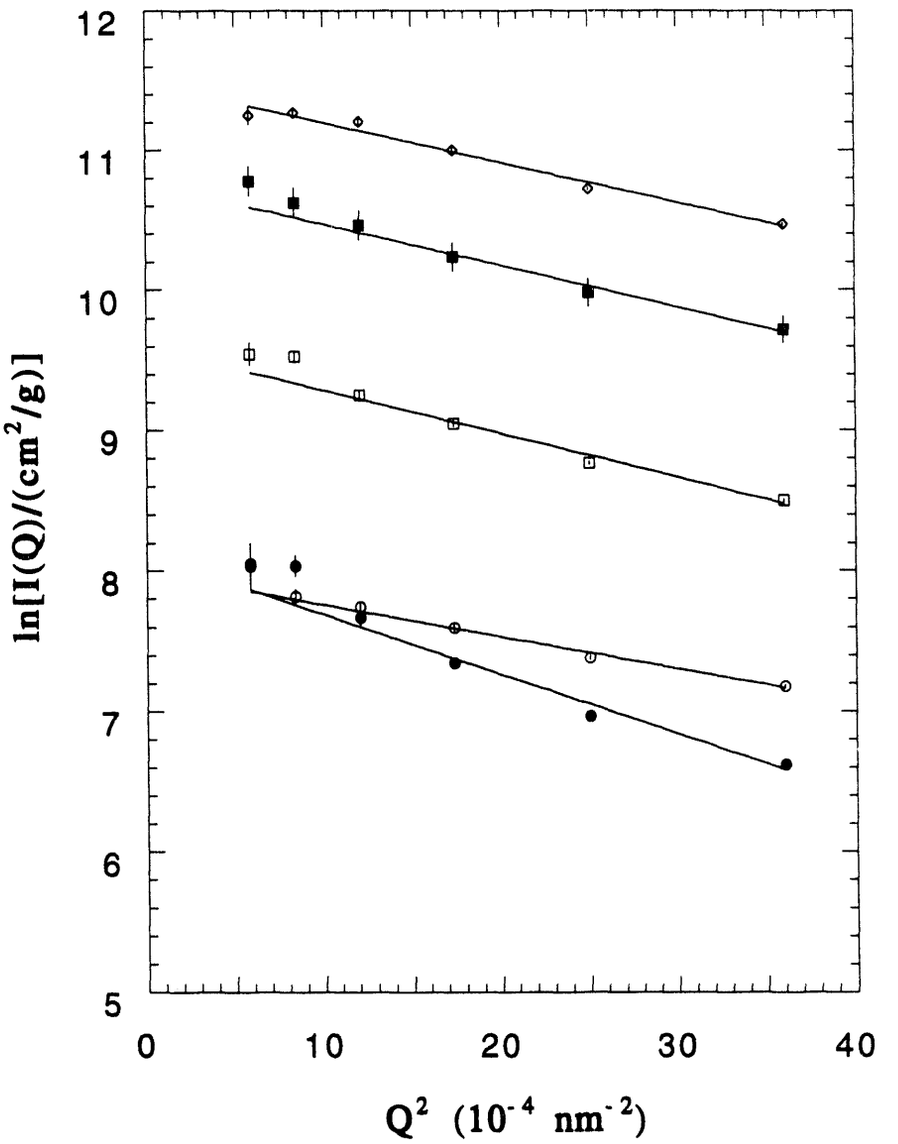

Fig 4

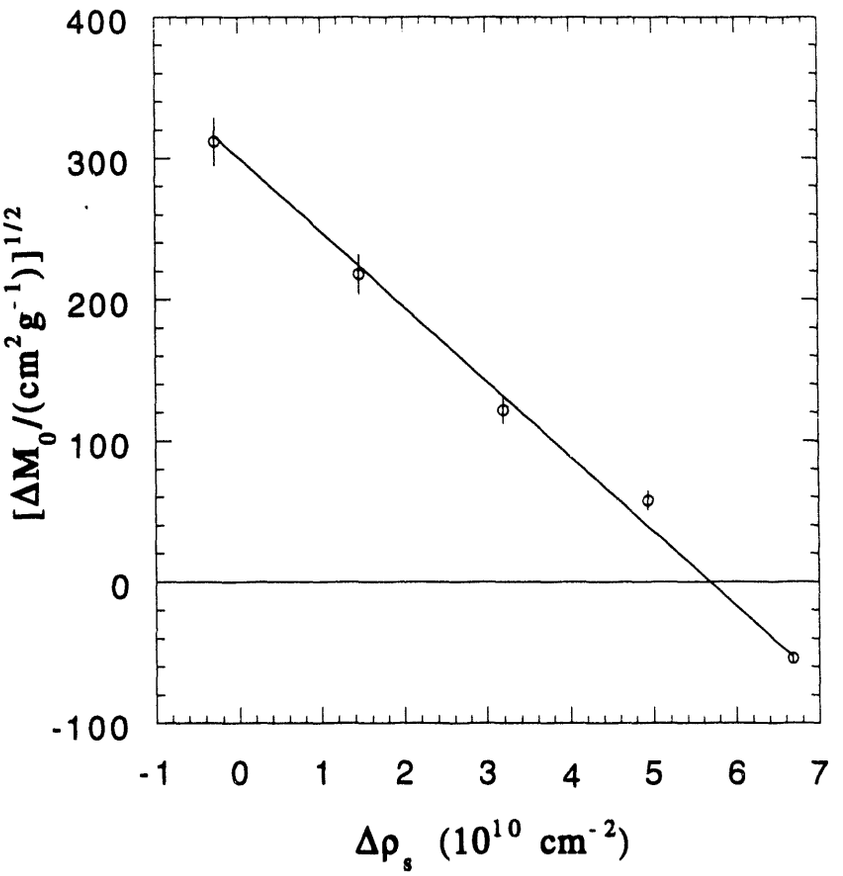
400
300
200
100
0
-100
-1
0
1
2
3
4
5
6
7
$[\Delta M_0/(cm^2 g^{-1})]^{1/2}$
$\Delta\rho_s$ $(10^{10}$ $cm^{-2})$

Fig 5

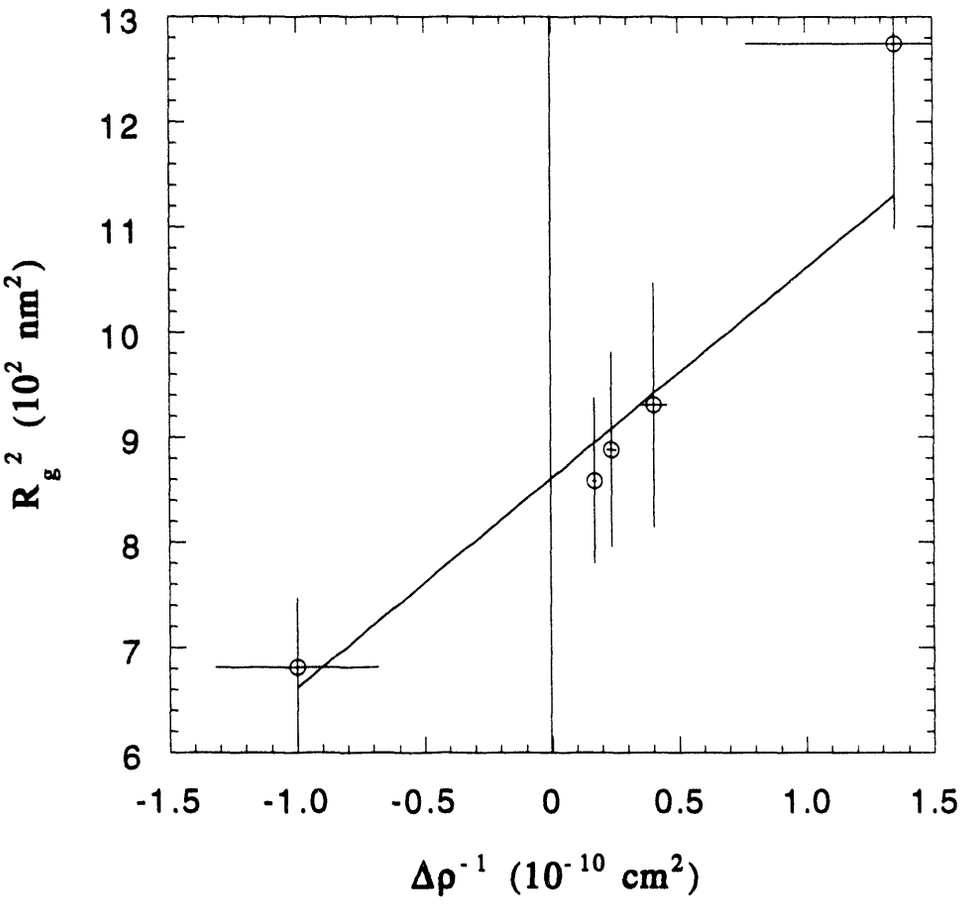
13
12
11
10
9
8
7
6
-1.5
-1.0
-0.5
0
0.5
1.0
1.5
R_g^2 (10^2 nm^2)
$\Delta\rho^{-1}$ (10^{-10} cm^2)

Fig 6

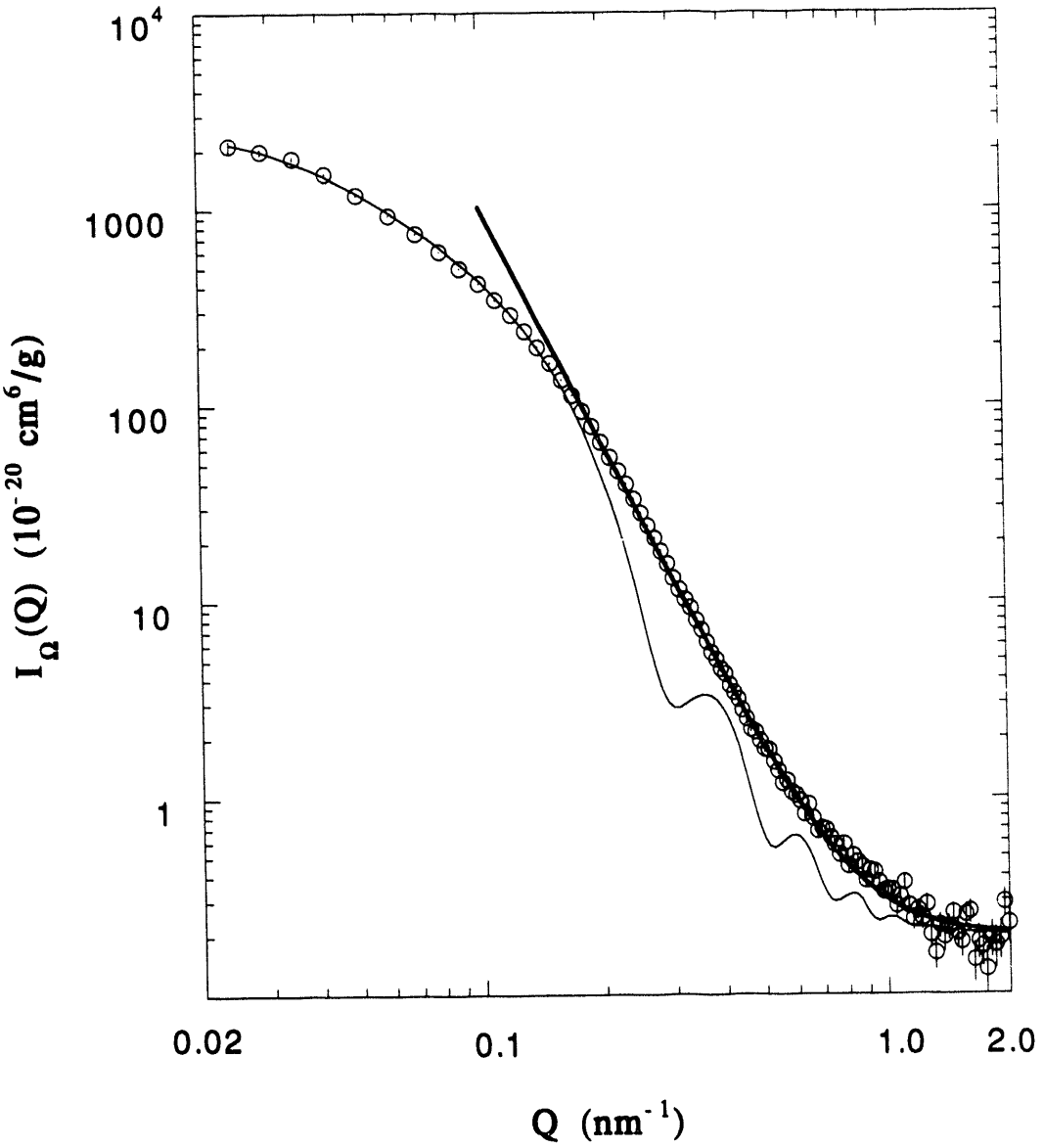

Fig 7

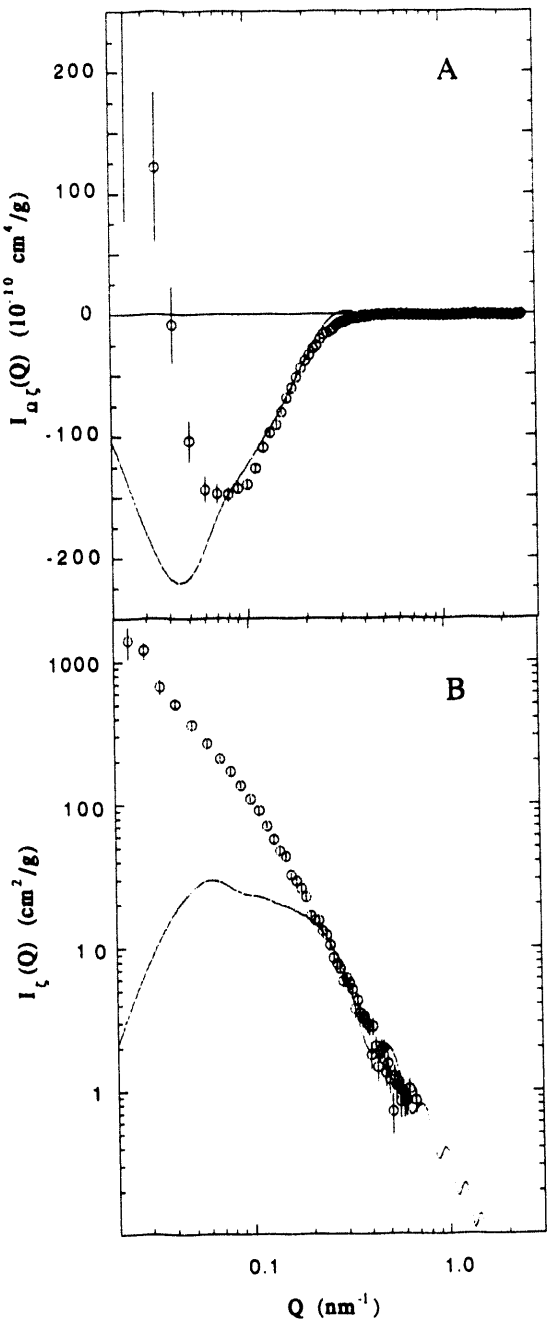
A
B
200
100
0
-100
-200
1000
100
10
1
0.1
1.0
$I_{\alpha\zeta}(Q)$ (10^{-10} cm^4/g)
$I_\zeta(Q)$ (cm^2/g)
Q (nm^{-1})

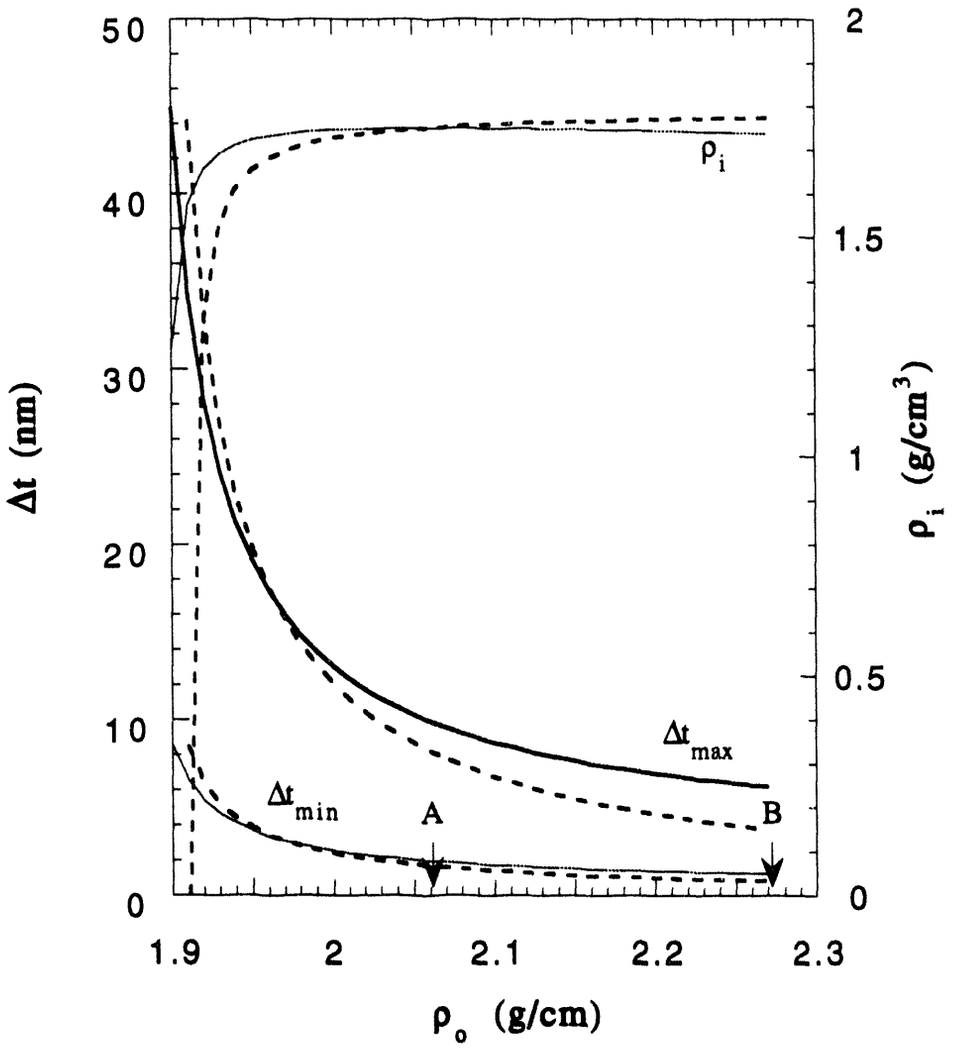
50
40
30
20
10
0
2
1.5
1
0.5
0
1.9
2
2.1
2.2
2.3
Δt (nm)
ρi (g/cm3)
ρo (g/cm)
ρi
Δtmax
Δtmin
A
B

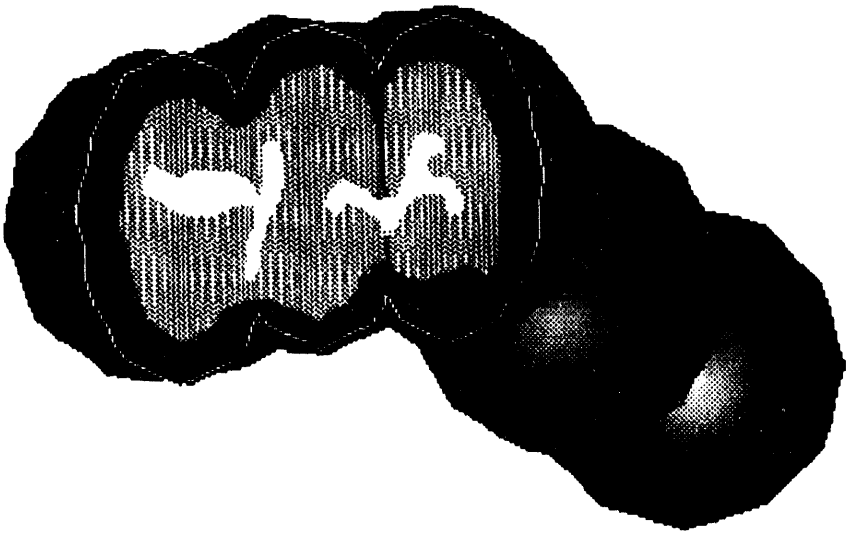

DATE
FILMED
4/29/94
END